# Tracking hole localization in *K*-shell and core-valence-excited acetylene photoionization via body-frame photoelectron angular distributions

T. N. Rescigno,[1] C. S. Trevisan,[2] and C. W. McCurdy[1,3]

[1]*Lawrence Berkeley National Laboratory, Chemical Sciences, Berkeley, California 94720, USA*

[2]*Department of Sciences and Mathematics, California Maritime Academy, Vallejo, California 94590, USA*

[3]*Department of Chemistry, University of California, Davis, California 95616, USA*

(Received 3 January 2015; published 25 February 2015)

Asymmetry in the molecular-frame photoelectron angular distributions from core-hole- or core-valence-excited polyatomic targets with symmetry-equivalent atoms can provide direct evidence for core-hole localization. Using acetylene as an example, we contrast the small asymmetry that can be seen in direct core-level ionization, due to the competition between two competing pathways to the continuum, with ionization from core-valence-excited HCCH, which offers the prospect of observing markedly greater asymmetry.

DOI: 10.1103/PhysRevA.91.023429 PACS number(s): 33.80.−b

## I. INTRODUCTION

Ever since Bagus and Schaefer [1] first observed that a considerably lower self-consistent-field energy could be obtained for a core-hole-ionized state of $O_2^+$ by relaxing the restriction that the orbitals have $g$ or $u$ symmetry, the subject of core-hole localization in molecules possessing symmetry-equivalent atoms has continued to attract the attention of theorists and experimentalists. For diatomic molecules, the question of whether core ionization creates a $1s$ hole in one of the atoms or a delocalized hole that preserves the symmetry of the molecule is still being debated. Indeed, experiments in which photoelectrons and Auger electrons produced by core ionization were measured in coincidence in the molecular frame demonstrated that in some cases the $K$-shell hole behaves like a localized state while in others as a delocalized one, depending on the angle of detection [2].

The situation in polyatomic molecules with symmetry-equivalent atoms is more straightforward, since the presence of asymmetric vibrational modes leads to a vibronic coupling between $g$ and $u$ states and the rapid localization of an initially created $K$-shell hole on a single atom [3]. Evidence for this mechanism has been seen in the case of acetylene, where there is rich vibrational fine structure in the C $(1s)^{-1} \rightarrow \pi^*$ band that is well described by a theoretical model which treats vibronic coupling in both the core and valence orbital spaces with broken-symmetry orbitals [4].

It has also been suggested that the asymmetry observed in molecular-frame $K$-shell photoelectron angular distributions (MFPADS) in molecules with symmetry-equivalent atoms provides direct evidence for core-hole localization. MFPADs for O $(1s)^{-1}$ ionization in $CO_2$ [5] and C $(1s)^{-1}$ ionization in HCCH [6], measured in coincidence with ion fragments that are produced after fast Auger decay into an asymmetric dissociation channel (e.g., $O^+ + CO^+$ in $CO_2$ and $H^+ + C_2H^+$ in HCCH), show definite asymmetry which has been ascribed to a localization of the core holes at geometries away from the symmetric equilibrium geometry. If Auger decay leading to asymmetric dissociation is fast relative to vibrational motion, then the memory of the instantaneous geometry at the moment of photon absorption is retained and imprinted on the asymmetric dissociation channel. However, it must be pointed out that, in the case of $CO_2$, asymmetry in the MFPAD is also observed for C $(1s)^{-1}$ ionization when measured in coincidence with the $O^+ + CO^+$ ion fragmentation channel [7,8]. Asymmetry associated with core-hole localization is a moot point in that case, since there is only a single carbon atom in the target. The observed asymmetry was quantitatively reproduced by considering the geometry dependence of the fixed-nuclei MFPADs which, when convoluted with the zero-point vibrational motion, explained the observed distributions [9]. So a question that naturally arises is to what extent core-hole localization enhances the geometry dependence of the MFPADs and, if it does, why the asymmetry observed in $CO_2$ for O $(1s)^{-1}$ ionization and in HCCH for C $(1s)^{-1}$ ionization is not markedly larger than that seen for C $(1s)^{-1}$ ionization in $CO_2$, which it is not. That question will be addressed here for the case of HCCH.

We will also examine an alternative, and potentially more decisive, way of using outer-valence MFPADs to observe hole localization in a small polyatomic, again using the acetylene molecule to illustrate the idea. An experiment would proceed in two steps. In the first step, a short x-ray pulse is used to excite, but not ionize, a core-valence state ($1s \rightarrow \pi^*$) below the carbon $K$ edge. Such a state typically lives for ∼6 fsec before it Auger decays, during which time the hole can localize on one of the carbon atoms. A second UV pulse then ionizes the excited $\pi^*$ valence electron before Auger decay can occur. If the angular distribution of the resulting photoelectrons is measured in the molecular frame in coincidence with ions produced in an asymmetric dissociation channel, a strong left-right asymmetry should be observed.

The outline of this paper is as follows. In the following section, we give a brief description of calculation of MFPADs using the complex Kohn formalism. In Sec. III, we describe the electronic structure calculations we performed to determine the target core-valence-excited states. Our calculated MFPADs are presented in Sec. IV. We conclude with a brief discussion.

## II. THEORY

### A. Molecular-frame photoionization cross sections

Photoionization cross sections in the molecular frame can be constructed from the matrix elements

$$I^{\mu}_{\Gamma_0} = \langle \Psi^-_{\Gamma_0} | r_\mu | \Psi_0 \rangle, \tag{1}$$

 

where $r_\mu$ is a component of the dipole operator, which we evaluate here in the length form,

$$r_\mu = \begin{cases} z, & \mu = 0, \\ \mp (x \pm iy)/\sqrt{2}, & \mu = \pm 1. \end{cases} \tag{2}$$

$\Psi^-_{\Gamma_0}$ is the final-state wave function for production of photoions in a specific cation state $\Gamma_0$ and $\Psi_0$ is the initial-state wave function of the neutral $N$ electron target. To construct an amplitude that represents an ionization process for a specific value of photoelectron momentum, $\mathbf{k}$, measured in the molecular body frame, we expand $\Psi^-_{\Gamma_0}$ in partial waves:

$$\psi^-_{\Gamma_0}(\mathbf{r}_1, \ldots, \mathbf{r}_N) = \sum_{l_0 m_0} i^{l_0} \exp\left(-i\delta_{l_0}\right) Y^*_{l_0 m_0} \times (\hat{\mathbf{k}}) \psi^-_{k,\Gamma_0 l_0 m_0}(\mathbf{r}_1, \ldots, \mathbf{r}_N), \tag{3}$$

with the Coulomb phase shift $\delta_{l_0}$ defined as

$$\delta_{l_0} = \arg \Gamma(l_0 + 1 - iZ/k). \tag{4}$$

The cross section, differential in the angle of photoejection and photon polarization relative to the fixed body frame of the molecule, is then given by

$$\frac{d^2\sigma}{d\Omega_{\hat{k},\Gamma_0} d\Omega_{\hat{\epsilon}}} = \frac{8\pi\omega}{3c} \left| I_{\hat{k},\Gamma_0,\hat{\epsilon}} \right|^2, \tag{5}$$

where $\omega$ is the photon energy, $c$ is the speed of light, and the amplitude $I_{\hat{k},\Gamma_0,\hat{\epsilon}}$ is given by

$$I_{\hat{k},\Gamma_0,\hat{\epsilon}} = \sqrt{\frac{4\pi}{3}} \sum_{\mu l_0 m_0} i^{-l_0} e^{i\delta_{l_0}} I^\mu_{\Gamma_0} Y_{1\mu}(\hat{\epsilon}) Y_{l_0 m_0}(\hat{k}). \tag{6}$$

At low photoelectron energies, molecular MFPADs reflect a competition between favored electron ejection along the direction of photon polarization or into regions favored by molecular environment, tempered by optical selection rules. To fill in the gaps dictated by optical selection rules, it is convenient to present the computational results at a particular nuclear geometry through an MFPAD integrated over all photon polarization directions [10]. This is obtained from Eqs. (5) and (6) by using the orthonormality of the spherical harmonics $Y_{1\mu}(\hat{\epsilon})$:

$$\int \frac{d^2\sigma}{d\Omega_{\hat{k}} d\Omega_{\hat{\epsilon}}} d\Omega_{\hat{\epsilon}} = \frac{8\pi\omega}{3c} \frac{4\pi}{3} \sum_\mu \left| \sum_{l_0 m_0} I^\mu_{\Gamma_0} Y_{l_0 m_0}(\hat{k}) \right|^2. \tag{7}$$

Equation (7) is the incoherent sum of the MFPADs over the three components of the dipole operator. This quantity must have the symmetry of the target cation state.

### B. Complex Kohn method

To compute the final-state wave function $\psi^-_{k,\Gamma_0 l_0 m_0}$, which describes the photoelectron escaping in the field of the residual molecular ion, we use the complex Kohn variational method [11,12]. In the present study, the wave function $\psi^-_{k,\Gamma_0 l_0 m_0}$ is expressed as

$$\psi^-_{k,\Gamma_0 l_0 m_0} = \hat{A}\left(\chi_{\Gamma_0} F^-_{\Gamma_0}\right) + \sum_i d^{\Gamma_0}_i \Theta_i \equiv P\Psi + Q\Psi, \tag{8}$$

where $\chi_{\Gamma_0}$ is the final $(N-1)$-electron ionic state, $F^-_{\Gamma_0}$ is the photoelectron continuum wave function, $\hat{A}$ is the antisymmetrization operator, and the $\Theta_i$ are $N$-electron correlation terms built from square-integrable functions.

In the Kohn method, the channel function $F^-_{\Gamma_0}$ is further expanded in terms of square-integrable functions plus numerical continuum functions as

$$F^-_{\Gamma_0} = \sum_i c^{\Gamma_0}_i \phi_i(r) + \sum_{lm} \sqrt{\frac{2}{\pi}} \left[ f_l(k_\Gamma, r) \delta_{ll_0} \delta_{mm_0} \delta_{\Gamma\Gamma_0} + T^{\Gamma\Gamma_0}_{ll_0 mm_0} h^-_l(k_\Gamma, r) \right] Y_{lm}(\hat{r})/(k_\Gamma r), \tag{9}$$

where $T^{\Gamma\Gamma_0}_{ll_0 mm_0}$ are elements of the $\mathbf{T}$ matrix, $\phi_i$ is a set of orthonormal (Cartesian-Gaussian) functions, and $f_l$ and $h^-_l$ are partial-wave continuum radial functions, behaving asymptotically as regular and incoming Coulomb functions:

$$\begin{aligned} &f_l(k_\Gamma, r \to \infty) \\ &\quad \longrightarrow \sin\left(k_\Gamma r + \frac{Z}{k_\Gamma} \ln 2k_\Gamma r - \frac{\pi l}{2} + \delta_l\right), \\ &h^-_l(k_\Gamma, r \to \infty) \\ &\quad \longrightarrow \exp\left[-i\left(k_\Gamma r + \frac{Z}{k_\Gamma} \ln 2k_\Gamma r - \frac{\pi l}{2} + \delta_l\right)\right]. \end{aligned} \tag{10}$$

By construction, the functions $\phi_i$, as well as the continuum functions $f_l$ and $h^-_l$, are chosen to be orthogonal to the molecular orbitals used to expand the initial target $\Psi_0$ and final ion state $\chi_{\Gamma_0}$. This constitutes a strong orthogonality constraint which must be relaxed by the inclusion of appropriate penetration terms $\Theta_i$ for every target molecular orbital that is not doubly occupied.

## III. BODY-FRAME ACETYLENE PHOTOIONIZATION

At its linear equilibrium geometry, neutral acetylene is nominally described by the electronic configuration $1\sigma_g^2\, 1\sigma_u^2\, 3\sigma_g^2\, 2\sigma_u^2\, 3\sigma_g^2\, 1\pi_4^4$ and, in linear geometry near equilibrium, by $1\sigma^2\, 2\sigma^2\, 3\sigma^2\, 4\sigma^2\, 5\sigma^2\, 1\pi^4$. The x-ray-absorption spectrum below the carbon $K$ edge at 291.1 eV is dominated by an intense peak at 285.8 eV [13] which results from promotion of a $1\sigma_g$ $(2\sigma)$ electron into the antibonding $1\pi_g{}^*$ $(2\pi^*)$ orbital. In the symmetric equilibrium nuclear configuration, the two equivalent C $1s$ sites give rise to quasidegenerate core orbitals $(1\sigma_g, 1\sigma_u)$ split by ~110 meV and thus a pair of core-valence $\Pi^*$ excited states of $g$ and $u$ symmetry, one dipole allowed $(^2\Pi_u)$ and one dipole forbidden $(^2\Pi_g)$ from the ground state. We turn our attention first to carbon $K$-shell ionization from neutral ground-state acetylene.

### A. *K*-shell photoionization

Adachi *et al.* [6] observed asymmetry in the MFPADs for HCCH $K$-shell ionization when the photoelectrons were measured in coincidence with fragment ions in the $H^+ + CCH^+$ dissociation channel. The measured asymmetry was largest (~10%) when the photon polarization was coincident with the molecular axis and, not surprisingly, vanished for perpendicular polarization. The observed asymmetry was attributed to core-hole localization. They argued that memory of

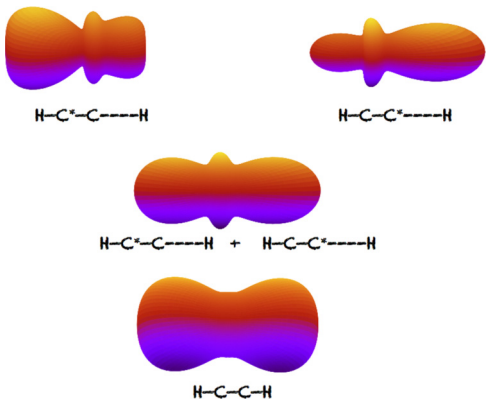


FIG. 1. (Color online) HCCH carbon $1s^{-1}$ MFPADs at 4 eV photoelectron energy averaged over photon polarization direction. Top: $1\sigma^{-1}$ and $2\sigma^{-1}$ components at rms asymmetric stretch geometry; asterisks label the carbon atom with the core hole. Middle: total MFPAD at asymmetric stretch geometry. Bottom: total MFPAD at equilibrium geometry. The MFPADs were rescaled to the same maximum magnitude.

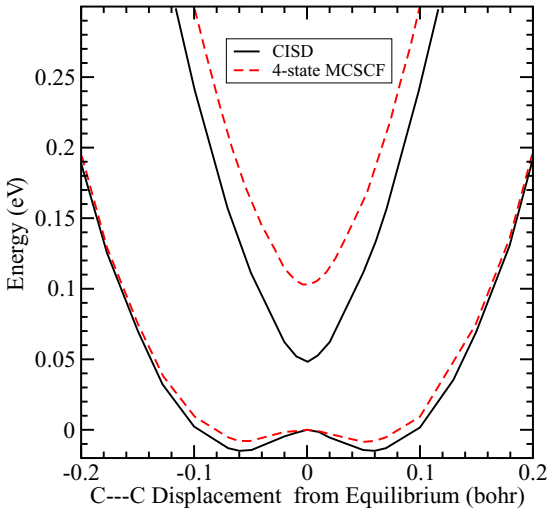


FIG. 2. (Color online) Potential-energy curves of the C $1s$-$\pi^*$ states of HCCH in linear geometry with the C–C distance fixed at its ground-state equilibrium value of 2.273 bohrs. Results are shown for four-state-averaged MCSCF and multireference CISD calculations.

the core-hole position in the ionized state can be communicated to the final dissociative state since the core-hole hopping time they calculated ($\tau_h \sim 40$ fs) was much greater than the Auger lifetime ($\tau_{\text{life}} \sim 7$ fs).

We have calculated the MFPADs for $K$-shell photoionization of HCCH using the formalism outlined above. The calculations were carried out in a two-state coupled-channel approximation using single-configuration wave functions for the $1\sigma^{-1}(1\sigma_g^{-1})$ and $2\sigma^{-1}(1\sigma_u^{-1})$ carbon $1s$ core-hole states constructed with neutral self-consistent-field molecular orbitals. The molecular orbitals were expanded in a Gaussian basis of $9s$, $6p$, and $1d$ carbon functions contracted to $5s$, $4p$, $1d$ and $10s$, $3p$ on the hydrogens, contracted to $5s$, $3p$. For the complex Kohn scattering calculations, the basis was augmented with additional diffuse functions—$3s$, $1p$ on the carbons and $2s$, $2p$ on the hydrogens. The calculations were done in linear geometry at an asymmetric configuration, using rms values for the CH bond distances in the $\nu = 0$ asymmetric stretch mode, and at equilibrium geometry as well. At the asymmetry geometry, the carbon $1\sigma$ and $2\sigma$ molecular orbitals are completely localized on the two carbon atoms. The results are shown in Fig. 1.

Evidently, the individual MFPAD components at asymmetric geometry display marked asymmetry, with increased propensity for photoelectron ejection on the side of the molecule where the core hole is localized. These components of the total MFPAD represent two quasidegenerate paths to the continuum. When summed, however, the resulting MFPAD shows only a small left-right asymmetry. The totally symmetric MFPAD at equilibrium geometry is also shown for comparison.

### B. Core-valence photoionization

We turn next to photoionization of the core-valence $\Pi^*$ states of acetylene. To characterize these states, we first carried out multireference configuration-interaction (MRCI) calculations, again restricting the calculations to linear geometries. A molecular-orbital basis for these calculations was obtained by starting with a self-consistent-field (SCF) calculation on neutral HCCH in an asymmetric linear geometry, which breaks the $g/u$ symmetry of the orbitals. The orbitals from this calculation were then used as a starting guess for a state-averaged multiconfiguration self-consistent-field (MCSCF) calculation on the doubly degenerate core-valence-excited $\Pi^*$ states. The MCSCF calculations were finally followed by a multireference singles and doubles configuration-interaction (CISD) calculation, using the four MCSCF configurations (i.e., $\Pi_{x,y}^{*,\text{lower}}$ and $\Pi_{x,y}^{*,\text{upper}}$) as reference configurations, with the restriction that there be at least one vacancy in either the $1\sigma$ or $2\sigma$ orbitals. MCSCF-CISD calculations were then carried out for a range of asymmetric stretch linear geometries, keeping the C-C distance fixed and using the MCSCF results from one geometry as a starting guess for the next. This procedure produced smooth adiabatic potential-energy curves for the $1s$-$\pi^*$ states with localized C $1s$ orbitals. The calculations were carried out using an augmented, correlation-consistent, polarized valence triple $\zeta$ basis with $11s, 6p, 3d, 2f$ functions on the carbons contracted to $5s$, $4p$, $3d$, $2f$ and $6s$, $3p$, $2d$ on the hydrogens contracted to $4s$, $3p$, $2d$. Results using this basis are plotted in Fig. 2. We find that the CISD calculations show a splitting of ~0.05 eV between the lower (dipole-allowed) and upper (dark) $\Pi^*$ states at the symmetric equilibrium geometry of ground-state HCCH. It is noteworthy that about the shallow potential wells in the lower state with minima near C–C displacements of $\pm 0.06$ bohr, the $1s$ hole localizes on the carbon atom opposite the stretched CH bond, while for the upper state at the same geometries the reverse is true. We also carried out similar calculations using the smaller basis previously described for core-hole ionization and found very similar results. Therefore, for the complex Kohn results, we used the smaller basis. The target $1s$-$\pi^*$ states for the photoionization calculations were carried out with single-configuration broken symmetry states constructed using natural orbitals from the CISD calculations.

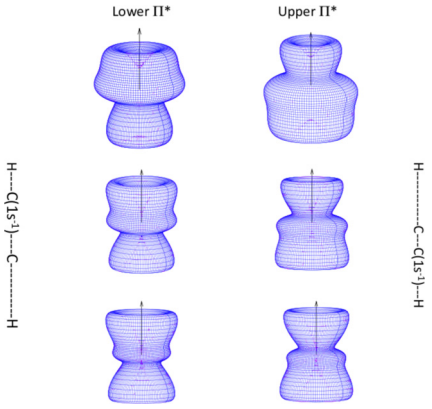


FIG. 3. (Color online) MFPADs for the lower (left) and upper (right) Π* states of HCCH at a C–C displacement of 0.06 bohr. MFPADs are averaged over all photon polarization directions and summed over degenerate components for each state. Results are for photoelectron energies of 2 eV (top), 4 eV (middle), and 6 eV (bottom).

MFPADs for both the lower and upper Π* states were calculated using single-configuration target neutral and ion states constructed from a common set of natural orbitals from the lower or upper Π* states, respectively. The MFPADs were averaged over all photon polarization directions and summed over the two degenerate components of each state. Figure 3 shows the results obtained for a C–C displacement of 0.06 bohr. A pronounced left-right asymmetry in the MFPADs is to be noted. The asymmetry tracks the position of the localized C 1*s* hole and is thus reversed for the lower and upper states.

Only the lower adiabatic Π* state is dipole-allowed from the ground state of HCCH. However, we must address the possibility that the dark upper state could be populated by vibronic interactions, which would then weaken the expected left-right asymmetry in the observed distributions since the asymmetry in the MFPADs for the lower and upper states would, when summed, cancel each other. To address this

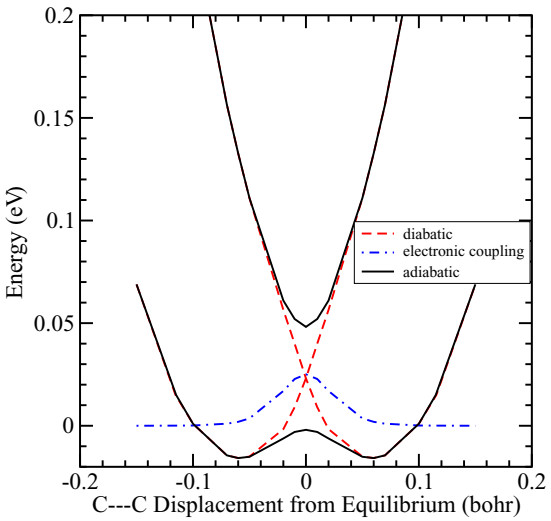


FIG. 4. (Color online) Diabatization of computed CISD potential-energy curves, following the treatment of Ref. [15].

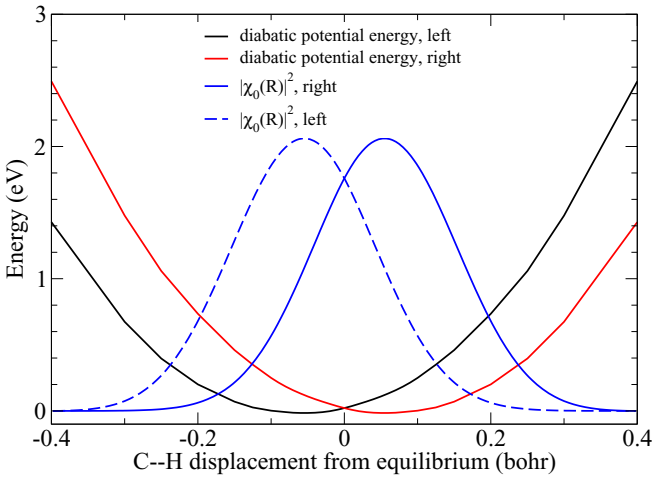


FIG. 5. (Color online) Vibrational $\nu = 0$ probability densities from two-state diabatic model.

effect, it is convenient to work in the diabatic representation, for which we use a two-state model in a simplified one-dimensional picture considering only the asymmetric stretch nuclear coordinate $R$ [14,15]. The diagonal adiabatic potential matrix $\mathbf{H}^a$, whose elements are the computed lower and upper Π* states, can be transformed into a diabatic potential matrix $\mathbf{H}^d$, whose diagonal elements are the diabatic potentials and the off-diagonal elements are the electronic coupling elements. The transformation is given by

$$\mathbf{H}^d = \mathbf{M}^{-1}\mathbf{H}^a\mathbf{M}, \tag{11}$$

with

$$\mathbf{M} = \begin{bmatrix} \cos\gamma(R) & -\sin\gamma(R) \\ \sin\gamma(R) & \cos\gamma(R) \end{bmatrix}. \tag{12}$$

The rotation angle $\gamma(R)$ can either be parametrized by following, for example, the procedure given by Roos, Orel, and Larson [15] or it can be evaluated *ab initio* from the computed nonadiabatic coupling $P_{12}$ using the relation [14]

$$\gamma(R) = \int_R^\infty P_{12}(R')dR'. \tag{13}$$

The computed diabatic potential curves and electronic coupling elements are shown in Fig. 4.

We used a two-state finite-element discrete variable representation method [16] to solve numerically for the vibrational wave functions using the computed potential-energy curves and electronic couplings. Figure 5 shows the probability density for the lowest vibrational levels computed in the diabatic representation. We note that the states are well localized over the left-right wells, so that MFPADs from these states should show the predicted asymmetry.

## IV. DISCUSSION

Using the acetylene case as an example, we have shown how two different classes of MFPADs, when measured in coincidence with an asymmetric fragment ion channel following Auger decay, can be used to observe core-hole localization in polyatomic molecules with symmetry-equivalent atoms. In the

case of direct core-level photoionization, the presence of two dipole-allowed pathways to the continuum corresponding to electron ejection from quasidegenerate core orbitals partially obscures the observed asymmetry in the total cross section. A potentially clearer picture of hole localization is obtained in a two-step process where an x-ray photon is first used to prepare a core-valence-excited state and a second UV photon is then used to ionize the species. The dark state can be suppressed by monitoring the ionization from the lowest vibrational levels of the core-excited states, since they are well localized and their MFPADs have marked left-right asymmetry.

The prospect for experimental observation of the effects discussed here will depend on the availability of short x-ray and UV pulse sources at the desired wavelengths and the ability to overlap these pulses in space and time. With pulses of 10 fs or longer, the effective bandwidths are less than 0.5 eV, so the shapes of the MFPADs should not be obscured by bandwidth issues. Some effort would be required to eliminate sources of background electrons of the same energy as the photoelectrons produced by sequential x-ray absorption and UV ionization. The C $1s^{-1}\pi^*$ state of acetylene lies at 285.8 eV and is the only strong x-ray absorption feature below the carbon $K$ edge at 291.1 eV. For the ionizing UV pulse, one would probably want to choose a laser frequency in the window between 6 and 8 eV—a range readily accessible by harmonic generation with an IR source—where there are no strong absorption bands in neutral acetylene and where the photionization signal from the $\Pi^*$ excited molecule is expected to be large. While a proposed experiment would no doubt be challenging, it should be feasible with the next generation of free-electron laser light sources.

## ACKNOWLEDGMENTS

This material is based upon work performed at the University of California Lawrence Berkeley National Laboratory and was supported by the US Department of Energy, Office of Science, Division of Chemical Sciences of the Office of Basic Energy Sciences under Contract No. DE-AC02-05CH11231.

[1] P. S. Bagus and H. F. Schaefer III, J. Chem. Phys. **56**, 224 (1972).
[2] M. S. Schöffler *et al.*, Science **320**, 920 (2008).
[3] W. Domcke and L. S. Cederbaum, Chem. Phys. **25**, 189 (1977).
[4] B. Kempgens *et al.*, Chem. Phys. Lett. **277**, 436 (1997).
[5] R. R. Lucchese, H. Fukuzawa, X.-J. Liu, T. Teranishi, N. Saito, and K. Ueda, J. Phys. B **45**, 194014 (2012).
[6] J. Adachi *et al.*, J. Phys. B **40**, F285 (2007).
[7] N. Saito *et al.*, J. Phys. B **36**, L25 (2003).
[8] X. -J. Liu *et al.*, Phys. Rev. Lett. **101**, 083001 (2008).
[9] S. Miyabe, C. W. McCurdy, A. E. Orel, and T. N. Rescigno, Phys. Rev. A **79**, 053401 (2009).
[10] C. S. Trevisan, C. W. McCurdy, and T. N. Rescigno, J. Phys. B **45**, 194002 (2012).
[11] T. N. Rescigno, B. H. Lengsfield III, and C. W. McCurdy, in *Modern Electronic Structure Theory*, edited by D. R. Yarkony (World Scientific, Singapore, 1995), Vol. 1, p. 501.
[12] T. N. Rescigno, B. H. Lengsfield III, and A. E. Orel, J. Chem. Phys. **99**, 5097 (1993).
[13] M. Tronc, G. C. King, and F. H. Read, J. Phys. B **12**, 137 (1979).
[14] J. Q. Sun and C. D. Lin, J. Phys. B **25**, 1363 (1992).
[15] J. B. Roos, A. E. Orel, and A. Larson, Phys. Rev. A **79**, 062510 (2009).
[16] T. N. Rescigno and C. W. McCurdy, Phys. Rev. A **62**, 032706 (2000).